Article

Photodetector Arrays Directly Assembled onto Polymer Substrates from Aqueous Solution

Fairland F. Amos, Stephen A. Morin, Jeremy A. Streifer, Robert J. Hamers, and Song Jin

J. Am. Chem. Soc., **2007**, 129 (46), 14296-14302• DOI: 10.1021/ja073675b • Publication Date (Web): 31 October 2007

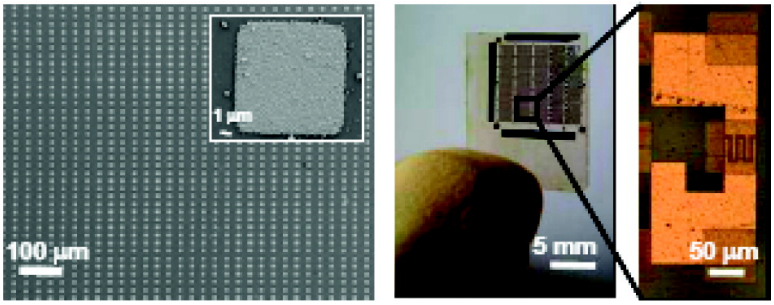

More About This Article

Additional resources and features associated with this article are available within the HTML version:

- Supporting Information
- Links to the 2 articles that cite this article, as of the time of this article download
- Access to high resolution figures
- Links to articles and content related to this article
- Copyright permission to reproduce figures and/or text from this article

View the Full Text HTML

J|A|C|S
ARTICLES
Published on Web 10/31/2007

Photodetector Arrays Directly Assembled onto Polymer Substrates from Aqueous Solution

Fairland F. Amos, Stephen A. Morin, Jeremy A. Streifer, Robert J. Hamers, and Song Jin*

Contribution from the Department of Chemistry, University of Wisconsin−Madison, Madison, Wisconsin 53706

Received May 22, 2007; E-mail: jin@chem.wisc.edu

Abstract: We report a simple and inexpensive approach to directly assemble arrays of cadmium sulfide (CdS) semiconductors onto transparent flexible poly(ethylene terephthalate) (PET) sheets via a polymer-mediated selective nucleation and growth process from an aqueous solution. This strategy of assembling functional materials onto plastics utilizes the surface functional molecules of the UV photooxidation patterned polymer to direct the nucleation and growth of CdS. We demonstrated that such assembled structures are viable for flexible macroelectronics, as manifested by the fabrication of CdS photodetector arrays on PET that can withstand bending. The best devices exhibited a specific detectivity of 3×10^{11} cm $Hz^{1/2}$ W^{-1} at 514-nm excitation wavelength at a modulation frequency of 90 Hz at room temperature. This direct assembly strategy eliminates additional lithography and etching steps during the deposition of the active inorganic semiconductor layer, is general to other inorganic materials and plastic substrates, and can enable low-cost, wearable, and/or disposable flexible electronics.

Introduction

The intense interest in exploiting plastics as substrates for macroelectronic applications stems from their advantages of flexibility, light weight, low cost, and roll-to-roll processing.[1−10] However, conventional semiconductor processing often limits the use of an assortment of organic substrates because of their chemical compatibility and thermal stability during the fabrication process. To address these challenges, current efforts in the fabrication of flexible devices often utilize a "transfer step" where previously prepared crystals or nanostructures are later assembled onto plastic sheets via a solution- or dry-processed fabrication using various methods, for example, Langmuir−Blodgett transfer,[11−13] solution-coating,[5−7] or stamping.[7−10] On the other hand, solution-based semiconductor synthesis and processing that have been studied since the 1970s[14−20] are highly compatible with polymer substrates because of the absence of high-temperature processing and the use of benign solvents in semiconductor formation and fabrication. However, patterning the functional materials that are synthesized from solution on the polymer sheets requires top-down fabrications and the subsequent chemical etching steps. Inspired by the biomineralization processes where organic matrices direct the nucleation, growth, and assembly of inorganic materials and control the location, size, and shape of the biominerals,[21−23] we herein report a simple and inexpensive approach to directly assemble arrays of cadmium sulfide (CdS) semiconductors onto transparent flexible poly(ethylene terephthalate) (PET) sheets via a polymer-directed selective nucleation and growth process via an aqueous solution and demonstrate photodetector device arrays with them.

In this approach, the directed assembly of a crystalline functional material onto a plastic substrate is incorporated during the nucleation and solution growth of the semiconductor and also just the required amount of functional materials is as-

(1) Cain, O. J. *Thin Solid Films* **1968**, *2*, 479.
(2) Rogers, J. A.; Bao, Z.; Baldwin, K.; Dodabalapur, A.; Crone, B.; Raju, V. R.; Kuck, V.; Katz, H.; Amundson, K.; Ewing, J.; Drzaic, P. *Proc. Natl. Acad. Sci. U.S.A.* **2001**, *98*, 4835.
(3) Nomura, K.; Ohta, H.; Takagi, A.; Kamiya, T.; Hirano, M.; Hosono, H. *Nature* **2004**, *432*, 488.
(4) Forrest, S. R. *Nature* **2004**, *428*, 911.
(5) Duan, X. F.; Niu, C. M.; Sahi, V.; Chen, J.; Parce, J. W.; Empedocles, S.; Goldman, J. L. *Nature* **2003**, *425*, 274.
(6) McAlpine, M. C.; Friedman, R. S.; Jin, S.; Lin, K. H.; Wang, W. U.; Lieber, C. M. *Nano Lett.* **2003**, *3*, 1531.
(7) Meitl, M. A.; Zhou, Y. X.; Gaur, A.; Jeon, S.; Usrey, M. L.; Strano, M. S.; Rogers, J. A. *Nano Lett.* **2004**, *4*, 1643.
(8) Sun, Y. G.; Rogers, J. A. *Nano Lett.* **2004**, *4*, 1953.
(9) Yuan, H.-C.; Ma, Z.; Roberts, M. M.; Savage, D. E.; Lagally, M. G. *J. Appl. Phys.* **2006**, *100*, 013708.
(10) McAlpine, M. C.; Ahmad, H.; Wang, D.; Heath, J. R. *Nat. Mater.* **2007**, *6*, 379.
(11) Jin, S.; Whang, D. M.; McAlpine, M. C.; Friedman, R. S.; Wu, Y.; Lieber, C. M. *Nano Lett.* **2004**, *4*, 915.
(12) Friedman, R. S.; McAlpine, M. C.; Ricketts, D. S.; Ham, D.; Lieber, C. M. *Nature* **2005**, *434*, 1085.
(13) Acharya, S.; Panda, A. B.; Belman, N.; Efrima, S.; Golan, Y. *Adv. Mater.* **2006**, *18*, 210.
(14) Pavaskar, N. R.; Menezes, C. A.; Sinha, A. P. B. *J. Electrochem. Soc.* **1977**, *124*, 743.
(15) Nair, P. K.; Campos, J.; Nair, M. T. S. *Semicond. Sci. Technol.* **1988**, *3*, 134.
(16) Hu, H. L.; Nair, P. K. *J. Cryst. Growth* **1995**, *152*, 150.
(17) Gan, F. Y.; Shih, I. *IEEE Trans. Electron Devices* **2002**, *49*, 15.
(18) Mitzi, D. B. *J. Mater. Chem.* **2004**, *14*, 2355.
(19) Mitzi, D. B.; Kosbar, L. L.; Murray, C. E.; Copel, M.; Afzali, A. *Nature* **2004**, *428*, 299.
(20) Konstantatos, G.; Howard, I.; Fischer, A.; Hoogland, S.; Clifford, J.; Klem, E.; Levina, L.; Sargent, E. H. *Nature* **2006**, *442*, 180.
(21) Addadi, L.; Weiner, S. *Angew. Chem., Int. Ed.* **1992**, *31*, 153.
(22) Mann, S. *Nature* **1993**, *365*, 499.
(23) Aksay, I. A.; Trau, M.; Manne, S.; Honma, I.; Yao, N.; Zhou, L.; Fenter, P.; Eisenberger, P. M.; Gruner, S. M. *Science* **1996**, *273*, 892.

10.1021/ja073675b CCC: $37.00

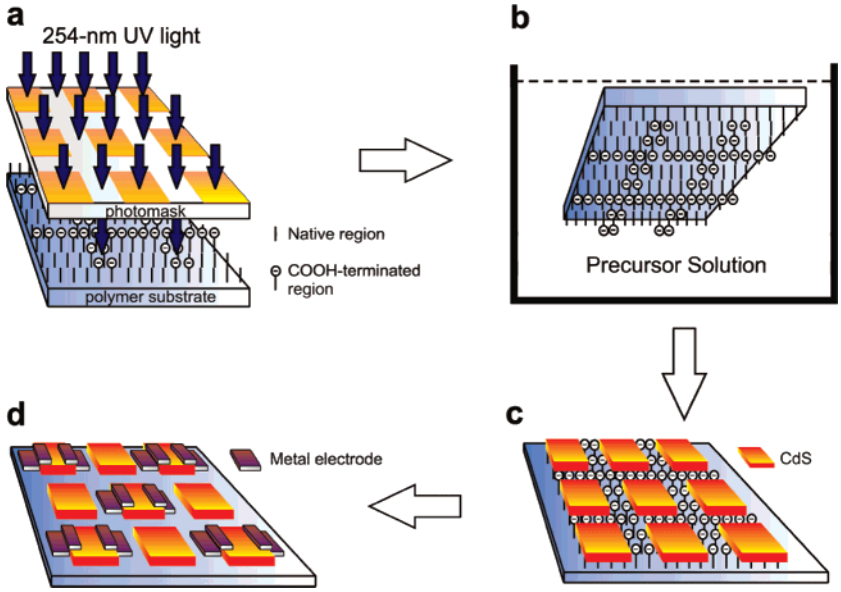

Figure 1. Schematic diagram for the direct assembly of CdS on polymer substrates and the fabrication of CdS-based flexible electronic devices. (a) Selective photooxidation of PET using 254-nm UV light to produce patterned surface carboxylic acid groups. (b) Exposure of the selectively oxidized PET in an aqueous growth solution. (c) Directed nucleation of CdS films to form an array on the non-irradiated regions of the PET. (d) Deposition of In/Au metal contacts on the CdS films to form an array of photodetector devices.

sembled at the locations where the devices are subsequently fabricated. The key to the success of this assembly strategy is the introduction of differing surface organic functionalities on the polymer substrates, which can promote heterogeneous nucleation events in selective regions of the substrates and suppress nucleation events in the other areas.[21,23−25] Surface molecules in the form of self-assembled monolayers (SAMs) with varying functionalities on metal surfaces have been successfully utilized to direct the assembly of inorganic crystals of $CaCO_3$ (calcite),[24] PbS and ZnS,[25] ZnO,[26] and organic crystals of anthracene.[27] The use of the polymer substrates allows us to exploit the inherent surface functional groups of the polymer matrix to assemble semiconducting or other functional materials directly. Furthermore, the *insulating* polymer substrate backplane, as opposed to the *metallic* substrates used in SAMs, enables the fabrication of electrical devices with these solution-assembled arrays. The strategy employed here eliminates the vacuum and high-temperature fabrication processes and the transfer step, therefore reducing the cost of device fabrication. Unlike traditional thin film processing, no additional chemical etching after lithography of the predeposited thin films is needed since the functional materials are already selectively patterned on the substrate through directed nucleation and growth.

Results and Discussion

Selective Polymer Surface Photooxidation. Our approach to device fabrication is illustrated in Figure 1. To introduce various patterned surface functionalities, PET was first irradiated with UV light in air under a photomask with square patterns (Figure 1a). Such UV irradiation is known to create carboxylic acid groups on the surface of the exposed regions of the polymer.[28] We first verify the surface functionalization of the

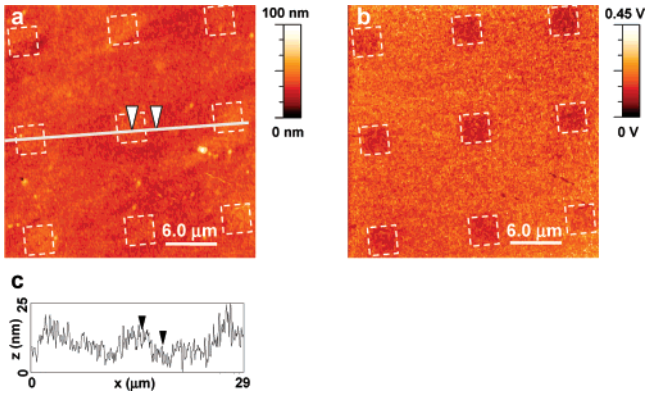

Figure 2. Lateral force micrographs of a selectively UV-irradiated PET substrate: (a) height and (b) friction mode images. The dashed squares in (a) and (b) highlight the non-irradiated regions of the polymer. (c) Height analysis of the sample across the irradiated and non-irradiated regions.

polymer using lateral force microscopy (LFM) in the height and friction modes; LFM is a modified AFM technique that analyzes the torsional force exerted on a slightly hydrophilized silicon nitride tip that is scanned at an angle of 90°.[29,30] The height mode image (Figure 2a) shows very little distinct physical changes across the polymer surface. Closer inspection reveals very slight topographical changes in the height and the roughness: the non-irradiated regions are slightly rougher (root mean square, rms, roughness, $R_q = 3.7 \pm 0.3$ nm) and more elevated (Figure 2c) than the irradiated regions ($R_q = 2.7 \pm 0.2$ nm). More importantly, the friction mode image (Figure 2b) reveals recognizable darker square patterns of approximately $4 \times 4\ \mu m^2$ each, corresponding to the areas blocked by the photomask during the UV exposure. These squares are darker because the frictional force between the hydrophilized Si_3N_4 tip and the non-irradiated hydrophobic polymer surface is smaller, whereas

(24) Aizenberg, J.; Black, A. J.; Whitesides, G. M. *Nature* **1999**, *398*, 495.
(25) Meldrum, F. C.; Flath, J.; Knoll, W. *Thin Solid Films* **1999**, *348*, 188.
(26) Hsu, J. W. P.; Tian, Z. R.; Simmons, N. C.; Matzke, C. M.; Voigt, J. A.; Liu, J. *Nano Lett.* **2005**, *5*, 83.
(27) Briseno, A. L.; Aizenberg, J.; Han, Y. J.; Penkala, R. A.; Moon, H.; Lovinger, A. J.; Kloc, C.; Bao, Z. A. *J. Am. Chem. Soc.* **2005**, *127*, 12164.
(28) Buxbaum, L. H. *Angew. Chem., Int. Ed.* **1968**, *7*, 182.
(29) Frisbie, C. D.; Rozsnyai, L. F.; Noy, A.; Wrighton, M. S.; Lieber, C. M. *Science* **1994**, *265*, 2071.
(30) Wilbur, J. L.; Biebuyck, H. A.; Macdonald, J. C.; Whitesides, G. M. *Langmuir* **1995**, *11*, 825.

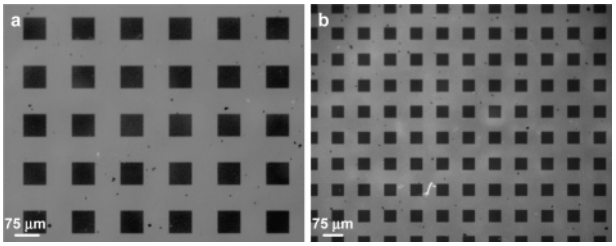

Figure 3. Fluorescent micrographs of the selectively UV-irradiated PET with (a) 75- and (b) 50-μm square patterns. The bright regions indicate the location of the surface carboxylic acid groups that are generated upon UV exposure and later labeled with 5-(aminoacetamido)fluorescein. The dark regions are the nonexposed, native PET.

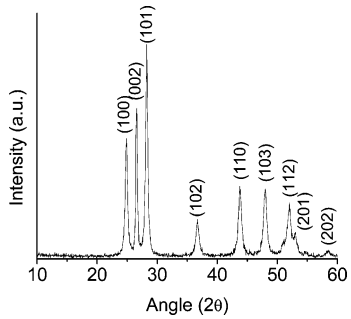

Figure 4. Powder X-ray diffraction of homogeneous solution-grown CdS. The diffraction peaks are indexed to the greenockite (wurtzite) structure (JCPDS 41-1049).

carboxylation of the irradiated regions makes the surface interact more strongly with the hydrophilic tip.

The selective carboxylation of the polymer due to UV exposure was further verified using fluorescence microscopy by specifically tagging the UV-generated carboxylic acid groups with a common fluorescent tag, 5-(aminoacetamido)fluorescein. Using a similar square pattern of the photomask used in Figure 2 (but with larger square sizes), we preferentially observed the fluorescent dye and thus the surface $-$COOH groups on the irradiated regions, as seen in the bright areas in the fluorescent micrographs (Figure 3). The non-irradiated regions, which retain the structure of the native polymer, remain unlabeled and dark under the fluorescent microscope. Figure 3 clearly shows a good edge resolution between the irradiated and the native regions of the polymer, which later translates into the formation of well-resolved patches of CdS.

Patterned CdS Film Formation. We then expose the selectively photooxidized PET films upside down in a growth solution of $CdCl_2$, thiourea, and hexamethylenetetramine (HMT) (see Experimental Section) at temperatures between 50 and 95 °C (Figure 1b), which results in the formation of polycrystalline CdS films on the native, unexposed regions of the PET (Figure 1c). CdS crystals are produced because the sulfide ions are released slowly from the decomposition of thiourea and react with the Cd^{2+} ions in solution.[14] Powder XRD confirms that these precipitates are of the wurtzite structure of CdS (Figure 4). We observed that the UV-irradiated regions, which have surface carboxylic groups, inhibit heterogeneous nucleation of CdS. This is similar to the previous observation that carboxyl-terminated SAMs suppress nucleation of ZnO microcrystals grown from aqueous solution.[26] It is possible that the Cd^{2+} ions complex with the surface carboxylic acid groups, thereby making the cations less readily available to react with the sulfide ions and suppressing the initial nucleation of the CdS crystallites.

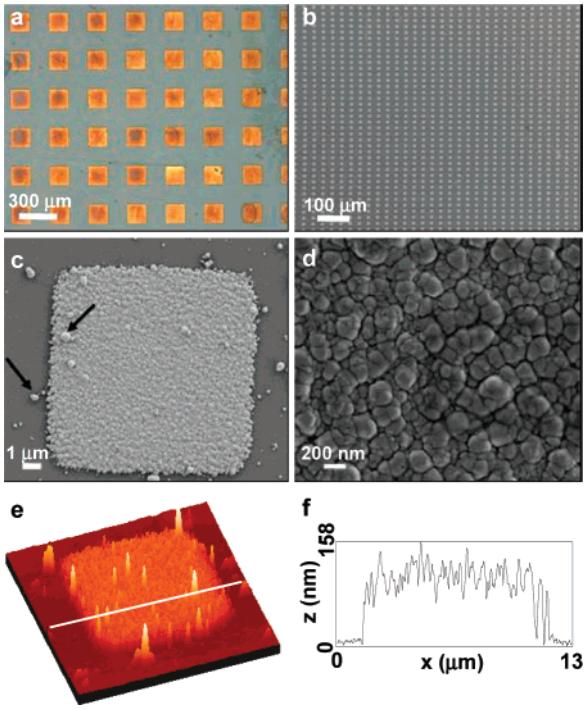

Figure 5. Arrays of polycrystalline CdS films of different sizes on PET substrate assembled from solution. (a, b) Optical and scanning electron images of two different arrays of CdS films assembled on the polymer. (c) A scanning electron micrograph of an individual CdS patch. Arrows point to the homogeneously grown CdS particles that are randomly deposited onto either PET or surface-nucleated CdS. (d) A higher magnification of (c) showing a dense and continuous film. (e) An atomic force micrograph of an individual CdS patch, and (f) its corresponding height profile.

In comparison, the native regions of the PET polymer surface are more suitable to allow deposition of the CdS film. The chemical contrast between the different regions is the most critical factor in differentiating the nucleation and growth, just as in the biomineralization processes, where the functional groups of organic matrix direct the nucleation of inorganic materials.[21,23] Figure 5a,b shows an assortment of arrays of polycrystalline CdS films formed on the PET sheets after multiple deposition cycles with the sizes of the arrays ranging from 4×4 μm^2 to 150×150 μm^2 and the periodicity of the arrays from 12 μm (for a 4×4 μm^2 square) to 300 μm (150×150 μm^2 square), as defined by the photomask design. The CdS nucleates and grows uniformly thoughout the non-irradiated regions of the PET (as opposed to an initial preferential nucleation along the border of the irradiated and non-irradiated regions of the polymer) and thickens gradually through each deposition cycle, as seen in a series of micrographs showing the patterned CdS film growth stopped and inspected at various stages of the growth process (Figure S1 in the Supporting Information). The arrays are deposited over the entire substrate, the total area of which is limited by the size of the polymer sheet employed. The individual CdS films are dense, compact, continuous (Figure 5c,d), and well-adhered on the polymer substrate even after sonication and multiple cycles of Scotch tape peel-off tests (Figure S2 in Supporting information) and thus suitable for the fabrication of thin film devices. Using AFM, we measured the height of these films to be approximately 150 nm (Figure 5e,f). Despite efforts to lessen the occurrence of the random attachment of homogeneously grown CdS (see Experimental Section), such deposition still occasionally occurs

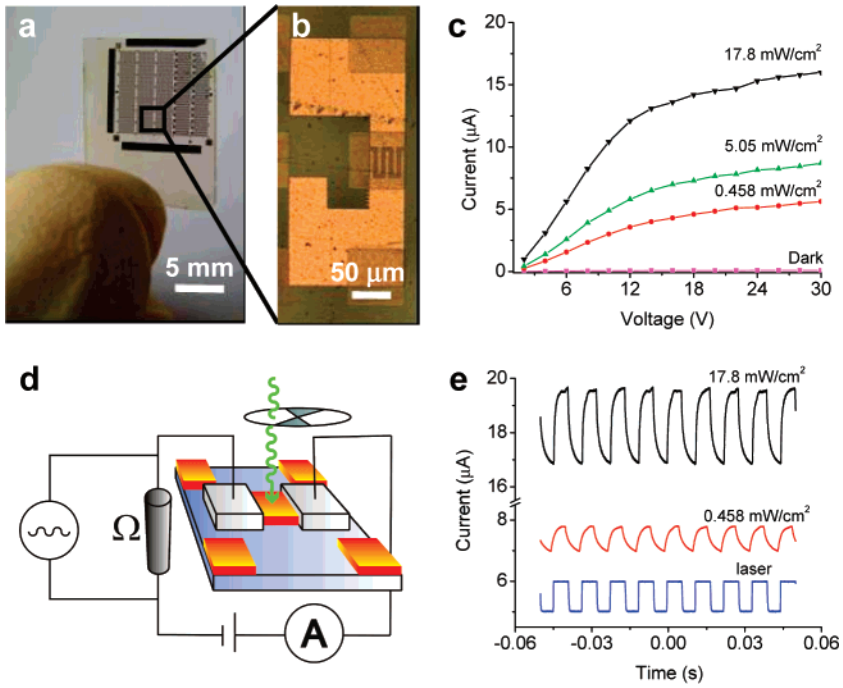

Figure 6. Arrays of photodetector devices based on CdS and characterization of the photoconducting properties. (a) An array of devices on the transparent flexible PET substrate. (b) An optical micrograph of a single photodetector device. (c) Dark and photocurrents at different irradiation power densities under a 514-nm laser static irradiation of a CdS film grown at 65 °C from the solution containing 10 mM $CdCl_2$, 4.3 mM HMT, and 15 mM thiourea. (d) Schematic diagram for the time-dependent signal current measurement using a chopper, a load resistor, a lock-in amplifier, an oscilloscope, and a source meter. (e) On−off switching of the CdS film grown in the same conditions as (c) using 514-nm laser chopped at 90 Hz at different power densities and a bias voltage of 60 V.

on the COOH-terminated PET regions or surface-nucleated CdS (arrows in Figure 5c). Although these particles are generally larger than the heterogeneously grown materials, consistent with previously reported homogeneously grown particles of CdS,[31] they do not pose any problems during device fabrication. Using very similar approaches, we have also preliminarily succeeded in assembling other functional inorganic materials, such as copper sulfide and nickel sulfide, into patterned thin films on PET substrates (Figure S3 in the Supporting Information).

Photodetector Devices. Using the arrays of CdS films assembled via this solution assembly approach, we have demonstrated low-cost and flexible macroelectronic devices on the insulating polymer back plane. CdS is an *n*-type semiconductor with a direct band gap of 2.4 eV and has excellent photoconducting properties in the visible spectrum range.[32] Metal electrode (In/Au) patterns are defined over these large-scale arrays of CdS films using photolithography (Figure 1d) to produce centimeter-scale CdS-based device arrays on the transparent PET sheet (Figure 6a). An optical micrograph of an individual photodetector device (Figure 6b) shows a 75 × 75 μm^2 patch of CdS film contacted by interdigitated In/Au electrodes. A typical photoconductive response of the CdS film that was grown from a solution containing 10 mM $CdCl_2$, 4.3 mM HMT, and 15 mM thiourea at 65 °C under 514-nm argon-ion static illumination at different power densities is shown in Figure 6c. The photocurrent passing through the CdS devices increases with increasing laser power. For instance, at a bias voltage of 30 V, the dark current passing through the film is 0.083 μA, whereas the photocurrent under a 17.8 mW/cm^2 irradiation is 16 μA, a 100-fold increase from the dark current. The time-dependent photoresponse of the CdS film was further investigated using the circuit diagram shown in Figure 6d with a 514-nm laser chopped at 90 Hz. The response using the same CdS device analyzed in Figure 6c under different laser power is shown in Figure 6e. At a low laser power density of 0.458 mW/cm^2, the peak-to-peak current (I_{pk-pk}) is 0.9 μA at a bias voltage of 60 V. At a higher irradiance of 17.8 mW/cm^2, I_{pk-pk} at the same voltage is 2.8 μA. In addition to the increase of I_{pk-pk} with increasing laser power, the DC current also increases because of either a rise in the density or the mobility of the charge carriers,[33] consistent with the previously reported photoconducting behavior of single and polycrystalline CdS.[34,35]

It can also be readily seen from Figure 6e that the OFF current under the dynamic irradiation at a high laser power does not return to the same level as the OFF current at low laser power irradiation. This has been previously attributed to the trapping of the photogenerated holes, which slows down the recombination with the free electrons and increases the majority carrier lifetime.[15,36] These trap sites can be reduced, and thus the recombination of electrons and holes increased with an increase in the thiourea concentration, as seen in the time-dependent response of a photodetector device shown in Figure 7, where the CdS film was synthesized from a solution containing 10 mM $CdCl_2$, 4.3 mM HMT, and 37.5 mM thiourea at 65 °C. Note that the OFF currents for both high power (17.8 mW/cm^2) and the low power (0.458 mW/cm^2) irradiation in Figure 7 are almost at the same level, which indicates that the recombination of the free electrons and holes readily occurs.

(31) Lincot, D.; Borges, R. O. *J. Electrochem. Soc.* **1992**, *139*, 1880.
(32) Kruse, P. W.; McGlauchlin, L. D.; McQuistan, R. B. *Elements of Infrared Technology: Generation, Transmission, and Detection;* Wiley & Sons: New York, 1962.
(33) Bube, R. H. *Annu. Rev. Mater. Sci.* **1975**, *5*, 201.
(34) Frerichs, R. *Phys. Rev.* **1947**, *72*, 594.
(35) Kuwabara, G. *J. Phys. Soc. Jpn.* **1954**, *9*, 97.
(36) Lambe, J. *Phys. Rev.* **1955**, *98*, 985.

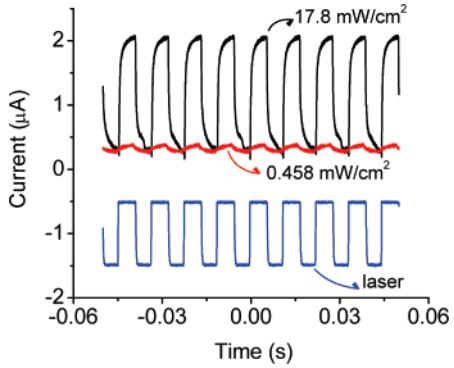

Figure 7. Time-dependent photoconductor response of a CdS film grown from a solution containing 10 mM $CdCl_2$, 4.3 mM HMT, and 37.5 mM thiourea at 65 °C under different power densities of the laser and 60-V bias voltage. The D^* values are 9.9×10^{10} and 3.0×10^{11} cm $Hz^{1/2}$/W for 17.8 and 0.458 mW/cm^2, respectively.

Enhancement of the Photodetector Performance. The performance of the CdS photodetectors is evaluated by determining the specific detectivity (D^*), which is defined as

$$D^* = \frac{I_s}{I_n H A_d} * (A_d \Delta f)^{1/2}$$

where I_s is the rms signal current due to the irradiation of the photoconductor with the 514-nm laser chopped at a 90-Hz frequency, I_n is the rms noise current, H is the irradiance, A_d is the active area of the detector defined by the electrode configuration, and Δf is the equivalent noise bandwidth. D^* is normalized to the active detector area (A_d) and the equivalent noise bandwidth (Δf) and is commonly used as a materials figure of merit describing the photoconductor sensitivity.[37] For example, the D^* for the CdS sample shown in Figure 6e at low laser power is 1.1×10^{11} cm $Hz^{1/2}$ W^{-1}. Because of the normalization to active areas, D^* for the same type of CdS film is not significantly different between different photodetector electrode configurations, such as simple square electrode gaps and interdigitated electrode patterns (Figure S4 and Table S1 in the Supporting Information).

To improve D^*, we investigated the effects of the synthetic conditions, mainly the growth temperature and the ratio of the thiourea to cadmium ions, which increase the I_s or decrease the I_n. At a constant temperature of 65 °C, an increase in the thiourea concentration results in a decrease in the dark current (or increase in the resistance, R, of the film) (Figure 8a). This suggests that sulfur vacancies, which contribute to the carrier concentration of the *n*-type CdS films, are reduced with the introduction of more sulfur precursor during growth. There is also an associated reduction in I_n with the increase of thiourea, as seen in Figure 8b. When the thiourea concentration is held constant at 15 mM, a decrease in synthesis temperature results in a decrease in both dark current (Figure 8c) and I_n (Figure 8d). This is likely due to the slower precipitation and loose packing of the CdS grains during a lower temperature synthesis compared to the higher-temperature deposition, which can result in a less direct charge carrier path across the films and a higher R. Lower temperature formation of CdS generally produces fewer precipitates, and therefore an adjustment in the deposition cycle had to be made during the synthesis at different temperatures. To produce ~150-nm-thick samples, the synthesis at 95 °C required changing the growth solution twice every 30 min, while at 50 °C the synthesis required solution replacement four or five times every 12 h.

The decrease in I_n is accompanied by a less pronounced decrease in I_s. Therefore, this leads to an improvement in the signal-to-noise ratio and D^*. Figure 9 shows the D^* as a variant of the thiourea concentration (5−15 mM) and synthesis temperature (50−95 °C). In general, D^* increases with a rise in the thiourea concentration and a decrease in the synthesis temperature except for samples grown at 95 °C, in which the trend is not very consistent for reasons yet unknown. The best D^* among the CdS photodetectors we examined here is 2.1×10^{11} cm $Hz^{1/2}$ W^{-1}, which is observed for the sample grown at a thiourea concentration of 15 mM and a temperature of 50 °C. A higher thiourea concentration (37.5 mM thiourea at 65 °C) was examined to further decrease the I_n value (as predicted by Figure 8a) and increase D^*. Even though the resulting D^* is slightly higher at 3.0×10^{11} cm $Hz^{1/2}$ W^{-1} (for an irradiation power of 0.458 mW/cm^2), the I_s at which the D^* is observed is too small to make such device practicably useful (Figure 7). In this device, the photocurrent at low irradiation is almost buried in the background current. A lower synthesis temperature of 40 °C was also attempted but this took a significant amount of deposition time (7 days) and did not yield films dense enough to allow for meaningful measurements of D^*. However, we do believe that the photoconducting properties of these CdS devices can be further improved since the measured noise current is still at least 2 orders of magnitude more than the theoretical shot noise limit (dashed lines in Figure 8b,d) and the estimated Johnson noise (plotted for each device in Figure 8b,d). Such enhancements should address the reduction of trap states associated with grain boundaries which are known to affect I_n in polycrystalline photoconductors[38] without possibly reducing I_s, and these may come from doping during film formation or low-temperature post-deposition treatments, such as halide, oxygen, or sulfur vapor exposure or other solution treatments.[39−41] Also, growing one microcrystal per surface nucleation site[24,26] can certainly enable essentially single-crystal device that can further enhance the device performance.

Implications for Flexible Macroelectronics. Although the D^* of these CdS photodetectors made from solution is modest compared to those high-temperature vacuum-processed CdS films (which have a reported D^* of 10^{13} cm $Hz^{1/2}$ W^{-1}),[32] their performance is adequate for many practical applications. We emphasize that our direct assembly approach offers many advantages over the high-temperature fabrication. One advantage is certainly the flexibility offered by the polymer substrate, which is easily incorporated during the solution-based assembly route employed here. The fabricated CdS-based devices on PET substrates were tested at various bending conditions to verify their function as flexible photodetectors. Figure 10a shows the photoconductor response of a representative CdS photodetector device before, during, and after it was subjected to bending at various radii of curvature ($r = 1.35$ and 0.95 cm) by taping the

(37) Jones, R. C. *Rev. Sci. Instrum.* **1953**, *24*, 1035.
(38) Carbone, A.; Mazzetti, P. *Phys. Rev. B* **1998**, *57*, 2454.
(39) Oigawa, H.; Fan, J. F.; Nannichi, Y.; Sugahara, H.; Oshima, M. *Jpn. J. Appl. Phys., Part 2* **1991**, *30*, L322.
(40) Chu, T. L.; Chu, S. S.; Schultz, N.; Wang, C.; Wu, C. Q. *J. Electrochem. Soc.* **1992**, *139*, 2443.
(41) Talapin, D. V.; Murray, C. B. *Science* **2005**, *310*, 86.

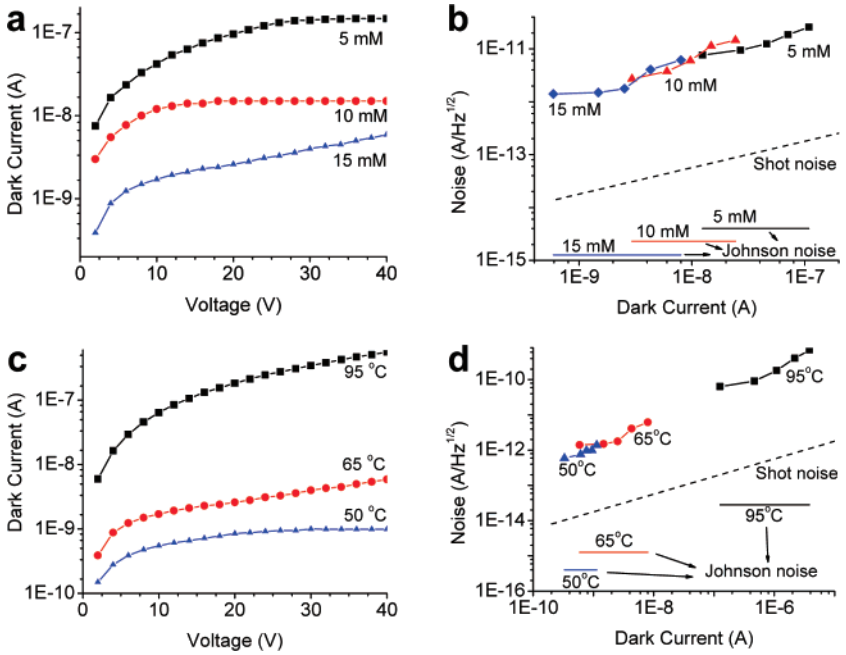

Figure 8. Performance of the CdS photodetectors at various experimental conditions. (a, b) Dark and noise currents at a constant synthesis temperature of 65 °C and various thiourea concentrations. (c, d) Dark and noise currents at a constant thiourea concentration of 15 mM and various synthesis temperatures. Dark current was measured directly on the CdS device without a load resistor. Noise current was measured through a 1 MΩ load resistor. Data points in (b) and (d) were measured for a given set of experimental conditions at 20-V increments. The shot noise, as well as the estimated Johnson noise for each of the device, is plotted for comparison with the experimental noise values in (b) and (d).

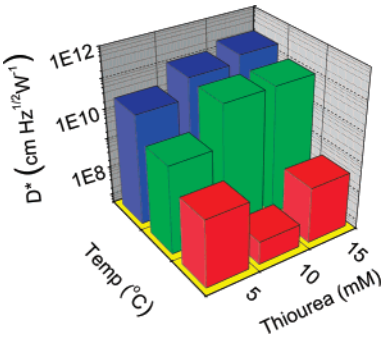

Figure 9. Specific detectivity of photodetector devices, *D**, as a function of the experimental conditions for the CdS films with thickness of about 150 nm.

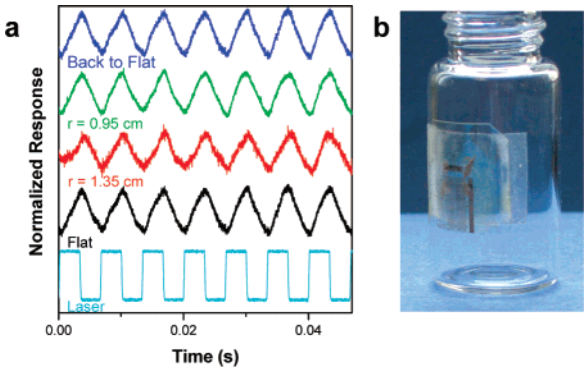

Figure 10. Flexible CdS photodetector response under various bending tests. (a) Time-dependent photoconductor responses (chopping frequency of 150 Hz) of a CdS device on PET substrate subjected to different radii of curvature. (b) A picture of a bent PET substrate that contain arrays of CdS devices taped around a glass vial with a 0.95-cm radius.

PET substrates to common glass vials (Figure 10b). No significant device deterioration or obvious CdS film cracking and peeling was observed in these bending tests, making this solution-based assembly approach a viable route in fabricating lower-cost flexible devices.

Furthermore, this solution-processed assembly uses simple, inexpensive, non-vacuum, and low-temperature synthesis in depositing and patterning the active semiconductor layer that complements the cheap substrate utilized in fabricating lower-cost devices. This synthetic route directly utilizes flexible polymer substrates and is highly compatible with continuous roll-to-roll processing through pulsed UV masking and solution chemical bath. No additional transfer, lithography, or post-deposition chemical etching steps are necessary to process the semiconductor layers further because the functional material with good physical properties is already selectively assembled or patterned onto the polymer substrate. Although more expensive methodologies of photolithography and metal evaporation are still employed in defining the metal electrodes for the devices, the overall process still represents a lower-cost route to the fabrication of large arrays of macroelectronic devices.

Conclusion

We have demonstrated a simple and inexpensive strategy to assemble functional materials onto flexible polymer substrates using surface functional molecules to guide the nucleation and growth directly from an aqueous solution. We have exploited such assembled structures for flexible macroelectronics, as exemplified by the fabrication of viable CdS photodetector arrays on flexible PET substrates with specific detectivity as high as 3×10^{11} cm $Hz^{1/2}$ W^{-1}. This general approach of assembling functional materials can be readily adapted to a wide variety of polymeric substrates with varying surface functionalities and complex or arbitrary shapes (e.g., fibers or spheres), as well as to a vast selection of solution-grown functional

inorganic materials in multiple layers to enable many other types of devices. This can potentially lead to the development of low-cost, flexible, wearable, and/or disposable technologies, limited not only to electrical devices but also to energy conversion and sensor applications.

Experimental Section

Materials and Chemicals. Sheets of PET (thickness = 0.2 mm), anhydrous cadmium chloride (≥99.0% pure), HMT (99%), thiourea (99.0%), and *N*-(3-dimethylaminopropyl)-*N*′-ethylcarbodiimide hydrochloride were purchased from Sigma-Aldrich. The fluorescent tag, 5-(aminoacetamido)fluorescein was purchased from Invitrogen Molecular Probes. These chemicals were used without further purification. Distilled deionized water was utilized in preparing the stock solutions. The plastic, cut to approximately 1.3 cm × 2.5 cm in size, was ultrasonically cleaned in water, acetone, and water successively for 10 min each and kept dry in an oven at 60 °C before use.

Assembly of CdS Arrays from Solution. Selective carboxyl functionalization was performed on the dried polymer sheets by placing them under a photomask and then irradiating them using a 254-nm UV light at 18.6 mW/cm^2 for 20 min under atmospheric conditions. The photooxidized PET sheets were placed upside down in an aqueous growth solution that contained 10 mM of $CdCl_2$, 4.3 mM of HMT, and various concentrations of thiourea at 50−95 °C. To minimize the random attachment of homogeneously grown CdS, the growth solutions were repeatedly replaced when they showed signs of yellow CdS precipitates. The solution exchange was repeated until a continuous dense film on the polymer was visible under an optical microscope (i.e., solution was changed twice every 30 min for deposition done at 95 °C; three or four times every 1 h at 65 °C; and four or five times every 12 h at 50 °C). In between the exchange, the polymer sheets were ultrasonicated in water for 10 s to further eliminate the homogeneously formed precipitates that are randomly adsorbed on PET. After the final deposition, the CdS-containing polymer was rinsed with ethanol and then N_2-dried.

Structural and Chemical Characterization. SEM images were taken using a LEO 1530 scanning electron microscope on samples that were sputter-coated with a thin layer of Au. LFM was carried out using a Digital Instruments Nanoscope IV atomic force microscope equipped with silicon nitride tip that was slightly hydrophilized using O_2 plasma at 10 W for 30 s. X-ray diffraction data was acquired using a STOE X-ray diffractometer from 10−60° (2θ) with a step size of 0.4°/min. Fluorescence microscopy was performed using a Nikon Eclipse ME600 fluorescence microscope on the selectively functionalized polymer substrates, where the carboxylic acid groups generated during photooxidation were labeled with a fluorescent tag 5-(aminoacetamido)-fluorescein by adapting a previously reported procedure.[42] Briefly, the selectively UV-irradiated polymer was placed in a reaction vessel containing a solution of 0.5 mM *N*-(3-dimethylaminopropyl)-*N*′-ethylcarbodiimide hydrochloride and 0.5 mM 5-(aminoacetamido)-fluorescein in 100 mM phosphate buffer at pH 7. The reaction vessel was sealed and allowed to shake slowly for 40 h in the dark. The polymer was then rinsed thoroughly with 100 mM phosphate buffer (pH 7) and then water and later dried with N_2 gas.

Photodetector Device Fabrication and Characterization. Interdigitated In (70 nm)/Au (70 nm) metal electrodes were defined on the resulting arrays of dense CdS film using standard photolithography and deposited using resistive (for In) and e-beam (for Au) evaporation. To connect the individual devices, copper wires were glued onto the metal electrodes using a conducting epoxy and later cured at 150 °C for 15 min. For photocurrent measurements, the 514-nm line of an argon-ion laser was attenuated with neutral density filters and expanded to irradiate the devices while a source voltage was applied directly to the photoconductor and the DC current was read from a Keithley 2400 source meter. Dark currents were measured on the device that had been kept in the dark for at least 12 h. For time-dependent measurements, the schematic circuit diagram shown in Figure 6d was used to determine the rms signal and noise currents. The load resistor used was 1 MΩ, and the chopping frequency was 90 Hz. Voltage was sourced through a Keithley 2400 source meter. Both I_s and I_n were read from the Stanford Research SR830 lock-in amplifier at a time constant of 1 s and a rolloff of 6 dB/oct. Specific detectivity was calculated using $D^* = [I_s/(I_n H A_d)]^*(A_d \Delta f)^{1/2}$, where I_s is the rms signal current due to the irradiation of the photoconductor with the 514-nm laser chopped at a 90-Hz frequency, I_n is the rms noise current, H is the irradiance, A_d is the active area of the detector defined by the electrode configuration (which is equal to 570 μm^2 for the interdigitated electrode design), and Δf is the equivalent noise bandwidth. Proper neutral density filters were chosen to attenuate H that would maximize I_s/H. For bending experiments, photocurrent measurements were carried out on the CdS devices grown from a solution containing 10 mM $CdCl_2$, 4.3 mM HMT, and 10 mM thiourea at 65 °C on polymer substrates that were taped on the outer surface of glass vials with various radii (r = 1.35 and 0.95 cm).

Acknowledgment. This research was supported by a SEED grant from the UW-Madison Nanoscale Science and Engineering Center (NSEC) (NSF DMR-0425880). S.J. also acknowledges the support from the 3M Nontenured Faculty Award and the DuPont Young Professor Grant.

Supporting Information Available: The evolution of the CdS film morphology through increasing deposition cycles, the adherence of the CdS films on the PET substrates analyzed using a simple Scotch tape peel-off test, the arrays of other functional inorganic materials on PET substrates grown from solution, and the comparison of D^* using different metal electrode configurations. This material is available free of charge via the Internet at http://pubs.acs.org.

JA073675B

(42) McCarley, R. L.; Vaidya, B.; Wei, S. Y.; Smith, A. F.; Patel, A. B.; Feng, J.; Murphy, M. C.; Soper, S. A. *J. Am. Chem. Soc.* **2005**, *127*, 842.